Atmospheric
Measurement
Techniques

Twin-cuvette measurement technique for investigation of dry deposition of O_3 and PAN to plant leaves under controlled humidity conditions

Shang Sun[1], Alexander Moravek[2], Lisa von der Heyden[3], Andreas Held[3,4], Matthias Sörgel[1], and Jürgen Kesselmeier[1]

[1]Max Planck Institute for Chemistry, Biogeochemistry Department, P.O. Box 3060, 55128 Mainz, Germany
[2]University of Toronto, Department of Chemistry, 80 St. George St, M5S 3H6, Toronto, Canada
[3]University of Bayreuth, Atmospheric Chemistry, 95440 Bayreuth, Germany
[4]University of Bayreuth, Bayreuth Center of Ecology and Environmental Research, 95440 Bayreuth, Germany

Correspondence to: Shang Sun (shang.sun@mpic.de)

Abstract. We present a dynamic twin-cuvette system for quantifying the trace-gas exchange fluxes between plants and the atmosphere under controlled temperature, light, and humidity conditions. Compared with a single-cuvette system, the twin-cuvette system is insensitive to disturbing background effects such as wall deposition. In combination with a climate chamber, we can perform flux measurements under constant and controllable environmental conditions. With an Automatic Temperature Regulated Air Humidification System (ATRAHS), we are able to regulate the relative humidity inside both cuvettes between 40 and 90 % with a high precision of 0.3 %. Thus, we could demonstrate that for a cuvette system operated with a high flow rate ($> 20\,\mathrm{L\,min^{-1}}$), a temperature-regulated humidification system such as ATRAHS is an accurate method for air humidification of the flushing air. Furthermore, the fully automatic progressive fill-up of ATRAHS based on a floating valve improved the performance of the entire measurement system and prevented data gaps. Two reactive gas species, ozone (O_3) and peroxyacetyl nitrate (PAN), were used to demonstrate the quality and performance of the twin-cuvette system. O_3 and PAN exchange with *Quercus ilex* was investigated over a 14 day measurement period under controlled climate chamber conditions. By using O_3 mixing ratios between 32 and 105 ppb and PAN mixing ratios between 100 and 350 ppt, a linear dependency of the O_3 flux as well as the PAN flux in relation to its ambient mixing ratio could be observed. At relative humidity (RH) of 40 %, the deposition velocity ratio of O_3 and PAN was determined to be 0.45. At that humidity, the deposition of O_3 to the plant leaves was found to be only controlled by the leaf stomata. For PAN, an additional resistance inhibited the uptake of PAN by the leaves. Furthermore, the formation of water films on the leaf surface of plants inside the chamber could be continuously tracked with our custom built leaf wetness sensors. Using this modified leaf wetness sensor measuring the electrical surface conductance on the leaves, an exponential relationship between the ambient humidity and the electrical surface conductance could be determined.

1 Introduction

The atmosphere–biosphere exchange of various trace gas species plays an important role for the climate and ecosystem interaction. The removal and emission of trace gases by the biosphere represents a significant factor, and its understanding is essential for atmospheric chemistry and the calculation of global trace gas budgets. While there is an increasing interest in the underlying mechanism of trace gas exchange of plants, various methods to determine the exchange flux of trace gases exist – in the field and under controlled laboratory conditions. For flux measurements on ecosystem level micrometeorological methods such as the eddy covariance or gradient method are used, causing only minimal disturbance (Horst and Weil, 1995). However, to understand the

Table 1. List of previous studies in the research field of O_3 and PAN flux measurement on plants under laboratory conditions.

Reference	Gas species	Plant species	Instrument	Method	Inlet mixing ratio	Regulated humidification	Deposition velocity mm s^{-1}
Fares et al. (2008)	O_3	*Quercus ilex, Populus nigra*	O_3-Analyzer Model 49	Plant chamber, gas phase reaction chamber	100 ppb	Not mentioned	0.9–1.8
Fares et al. (2010)	O_3	*Citrus limon, Citrus reticulata, Citrus sinensis*	O_3-Analyzer Dasibi mod. 1008-AH	Branch dynamic enclosure	40–160 ppb	No	2–5
Wang et al. (1995)	O_3	*Populus trichocarpa, Populus deltoides, Phaseolus vulgaris, Cucurbita sativus, Cucurbita pepo*	O_3-Analyzer Dasibi 1003	Single dynamic chamber (inlet & outlet measurement)	< 200 ppb	No	0.02–0.05
Van Hove et al. (1999)	O_3	*Populus nigra, P.brandaris, P.robusta*	O_3-Analyzer	Leaf chamber (inlet & outlet measurement)	30–100 ppb	No	–
Teklemariam and Sparks (2004)	PAN	*Zea mays, Triticum aestivum, Helianthus annuus, Catharanthus roseus*	GC (ECD) Limit 5 ppt, precision better than 1 % > 200 ppt	Single dynamic chamber (inlet & outlet measurement)	0.8–18 ppb	No	0.03–0.3
Okano et al. (1990)	PAN	*Herbaceous species*	2x GC (ECD) For inlet and outlet	Single dynamic chamber (inlet & outlet measurement)	190 ppb	No	0.3–3.1
Sparks et al. (2003)	PAN	*Zea mays, Phaseolus vulgaris, Pinus contorta, Mangifera indica, Quercus velutina, Quercus rubra, Abies grandis, Picea engelmannii*	GC (ECD) Limit 5 ppt, precision better than 1 % > 200 ppt	Single dynamic chamber (inlet & outlet measurement)	250 ppt	No	1.8–4.9
This study	PAN, O_3	*Quercus ilex*	O_3-Analyzer Model 49i, GC (ECD) LOD 1 ppt, precision 2 % < 800 ppt	Dual dynamic cuvette system (four position measurement)	O_3: 60 ppb PAN: 280 ppt	Yes 40–90 %	See Sect. 3.2.1

mechanism and processes in more detail, measurement on the plant and leaf scale under controlled environment conditions are often used. Therefore, enclosure techniques are mainly used to perform experiments under constant environmental conditions for investigation of the interaction between the plant and the atmosphere with higher resolution and reliability. For these experiments, it is important to minimize the disturbance of the environmental conditions such as radiation, humidity, temperature, and the trace gas concentration to ensure an optimum of plant physiological activity (Pape et al., 2009). Especially for flux measurements of trace gases whose exchange processes are predominantly controlled by

the leaf stomata, such reproducible preconditions should be achieved.

A commonly used technique for the measurement of trace gas uptake and release on plant and leaf scale is the dynamic cuvette technique (e.g., Breuninger et al., 2012). In the field, it can be ensured that the inner trace gas concentration and other related quantities are constant and close to the ambient conditions outside of the cuvette by the continuous renewal of the air inside the cuvette. For laboratory measurements, the dynamic cuvette leads to a temporally constant trace gas mixing ratio inside the cuvette. Typically, systems employ one single dynamic cuvette, in which the trace gas concen-

tration is measured at the entrance position of the cuvette and inside the cuvette to retrieve the trace gas flux. One disadvantage of such cuvette systems is the potential adsorption and/or desorption effects on the cuvette walls, which is critical, especially for reactive trace gases (Kulmala et al., 1999; Pape et al., 2009). Furthermore, the influence of humidity is an important factor for the surface deposition of various water soluble trace gas species (e.g., NH_3, SO_2, NO, NO_2, organic and inorganic acids and oxygenated monoterpenes such as linalool and 1,8-cineole) in the atmosphere (Kruit et al., 2008; Niinemets et al., 2011). Even substances with less water solubility (e.g., O_3) can be affected by higher air humidity resulting in a water film on the leaf surface (Altimir et al., 2006; Fuentes and Gillespie, 1992). In this paper, we present the use of a twin-cuvette system, which was designed to perform long-term flux measurements under controlled laboratory conditions. The setup is based on a cuvette system, which was previously used for measurements of volatile organic compounds (VOCs) and NO_2 (Kesselmeier et al., 1996; Chaparro-Suarez et al., 2011; Breuninger et al., 2012). To account for wall effects and other systematic uncertainties, a main feature of the system was the employment of a second, empty cuvette, which was used as a reference. To control the humidity in both cuvettes, we developed a new humidification system, which allowed for a precise regulation of the humidity inside the cuvettes. This allows to investigate important questions such as the relationship between humidity and the trace gas deposition on vegetation surfaces with high reliability. The twin-cuvette system was first developed for the plant–atmosphere exchange of PAN (peroxyacetyl nitrate) and O_3. While previous investigations mainly focused on the effect of inorganic nitrogen containing trace gases, particularly NO_2 to plants (Hill, 1971; Sparks et al., 2001; Ortega et al., 2008; Breuninger et al., 2012), studies on the uptake of gaseous organic nitrogen species such as PAN under laboratory conditions are rare. An overview is given in Table 1.

Laboratory studies which were designed to compare the PAN deposition with O_3 deposition have not been performed up to now (Table 5). Both Okano et al. (1990) and Teklemariam and Sparks (2004) used relatively high PAN mixing ratios (up to 190 ppb) for fumigation, which do not correspond to the PAN mixing ratios found under typical environmental conditions. Furthermore, the obtained deposition velocities in these studies differed considerably (see Table 1), which might be attributed to the use of different plant species and measurement methods. With adapting the cuvette conditions as closely as possible to the ones found in natural environments, our dual cuvette system is convenient for investigating the deposition mechanism of O_3 and PAN on plants concerning their reactivity and potential wall effect with plant surface as well as the wall material.

2 Material and methods

2.1 Setup of dual dynamic cuvette system

2.1.1 General setup

The experimental setup consisted of two dynamic cuvettes (Kesselmeier et al., 1996; Chaparro-Suarez et al., 2011; Breuninger et al., 2012) (see Figs. 1 and 2). The entire plant sample above the soil was introduced into the sample cuvette. The leaf temperature was measured by thermocouples (Type E, OMEGA Engineering. Inc., USA) at four different positions of the plant. Pressurized air flow was provided by a compressor and was purified by different filter cartridges filled with glass wool (Merck, Germany), silica gel (2–5 mm Merck, Germany), Purafil® ($KMnO_4/Al_2O_3$, Purafil Inc., USA) and active charcoal (LS – labor service, Germany), producing air free of O_3, NO, NO_2 and PAN. The purified air stream (20 L min^{-1} for each cuvette) was regulated by two mass flow controllers (MFC) (MKS Instruments, USA) and humidified to a predefined RH value (ATRAHS see, Sect. 2.1.3). The addition of O_3 and PAN into the main air stream occurred under atmospheric pressure downstream of the humidification step. To perform exchange flux measurements under controlled laboratory conditions, the pure air had to be enriched by known amounts of both O_3 and PAN. PAN was produced by a calibration unit (Meteorologie Consult GmbH, Germany) via gas phase photolysis of acetone in the presence of NO (see Sect. 2.3.2) (Patz et al., 2002). O_3 was produced by a primary standard device (Model 49C Primary Standard, Thermo Fisher Scientific, USA) via photolysis of O_2 in the synthetic air stream. A precise addition of the O_3 and PAN to the pure air stream was obtained by the use of MFCs. Both calibration devices had to be operated at atmospheric pressure at their outlet. Therefore, a Teflon membrane pump (KNF Neuberger GmbH, Germany) was implemented to deliver an over pressure of nearly 1.6 bar, which was needed to operate the MFCs (see Fig. 1, No. 11–15) for providing a controlled stream of the gas mixture to the system. With this additional setup, stable mixing ratio levels of O_3 and PAN within both cuvettes could be achieved. Downstream of the cuvettes, three Teflon-valves (Entegris, Inc. USA) were used to switch between inlet and outlet of both cuvettes for the analysis of O_3 and PAN mixing ratios (see Fig. 1, No. 9). The PAN mixing ratio was continuously measured by an automatic gas chromatograph with electron capture detection (GC-ECD) (Meteorologie Consult GmbH, Germany, see also Volz-Thomas et al., 2002). PAN was pre-concentrated over a duration of 5 min on a capillary column, which was thermally controlled at 2 °C. This enhanced the detection limit of the PAN analyzer to less than 5 ppt (see Sect. 3.1.1) and leads to PAN mixing ratios which represented average conditions over the 5 min period in contrast to a single point measurement. At the same time, the pre-concentration unit was operated in the saturation mode
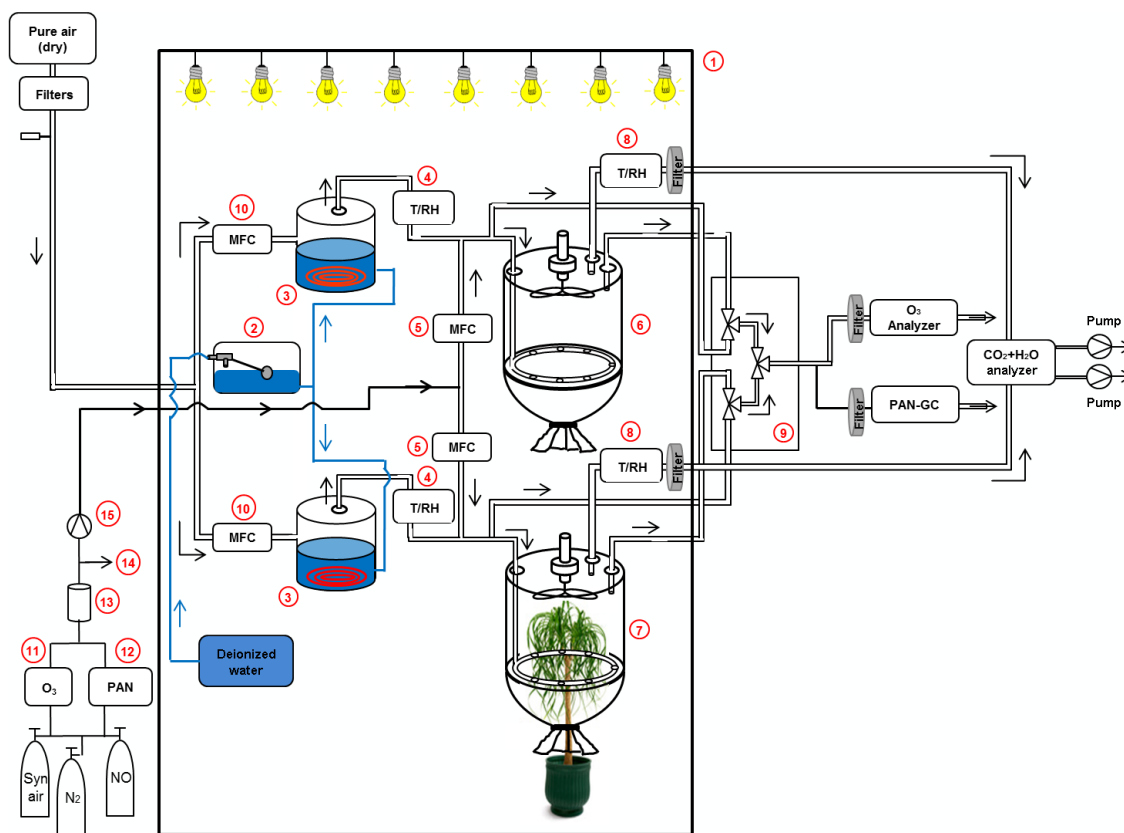
Figure 1. Flow chart of the dual cuvette system. 1 – plant cabinet; 2 – water storage tank (see Sect. 2.1.3); 3 – ATRAHS (see Sect. 2.1.3); 4 – Temperature and relative humidity sensor for humidity regulation (see Sect. 2.1.3); 5 – mass flow controller (MFC); 6 – dynamic cuvette (reference); 7 – dynamic cuvette (sample); 8 – temperature and relative humidity sensor for monitoring; 9 – Teflon-valve block; 10 – MFC for gas addition; 11 – O_3 – primary standard; 12 – PAN – calibration unit; 13 – mixing vessel; 14 – overflow; 15 – Teflon membrane pump.

to reduce the susceptibility to lower flow rate and pressure fluctuation (Moravek et al., 2014). The flow rate through the pre-concentration column was $9\,\mathrm{mL\,min^{-1}}$ to optimize the saturation time of the column. A Nafion dryer was used to prevent water condensation in the pre-concentration column. The design and characteristics of the pre-concentration unit is described in further detail elsewhere (Moravek et al., 2014). The O_3 mixing ratio was measured by a UV photometric analyzer (Model 49i, Thermo Fisher Scientific, USA). After inserting the plant into the sample cuvette, the relative difference of O_3 and PAN mixing ratios between the sample and the reference cuvette corresponded to O_3 and PAN uptake by the leaves, respectively. The valve switching between both cuvettes was controlled automatically with an interval of 10 minutes, which matched to the measurement cycle of the PAN GC-ECD. Inlet mixing ratios of both cuvettes were monitored once per hour over the entire experiment. Due to the pressure fluctuation at the moment of the valve switching only the data values between 30 s and 9 min 30 s of each measured position were averaged. The cuvettes were located inside a plant cabinet (VB1014, Vötsch GmbH, Germany) to keep the environmental temperature constant during the

experiments (see Sect. 2.2.2). The photosynthetic active radiation (PAR) was measured by a quantum sensor (Model LI-190SA, LiCor Inc., USA). In addition, CO_2 and H_2O concentrations were measured with an infrared gas analyzer (Li-7000, LiCor Inc., USA) to determine plant photosynthesis and transpiration. The Li-7000 operated in the differential mode to measure the concentration difference of CO_2 and H_2O between both cuvettes simultaneously.

2.1.2 Dynamic cuvettes

The wall material of the cuvettes was made of FEP foil (Saint Gobain Performance Plastics Corporation, USA) to minimize wall effects for the measured trace gases. All tubing and tubing connections that were in contact with the air flow consisted of PFA-Teflon® (Swagelok, USA). A fan (APC Propellers, USA), which had been coated with Teflon® by the MPIC mechanical workshop, was installed inside both cuvettes to assure well-mixed conditions in order to reduce the aerodynamic resistance for the trace gas fluxes (Gut et al., 2002). The purified air stream supplied with a certain mixing ratio of O_3 and PAN reached the inner cuvette through the inlet PFA-tube (see Fig. 2). With an additional perfo-
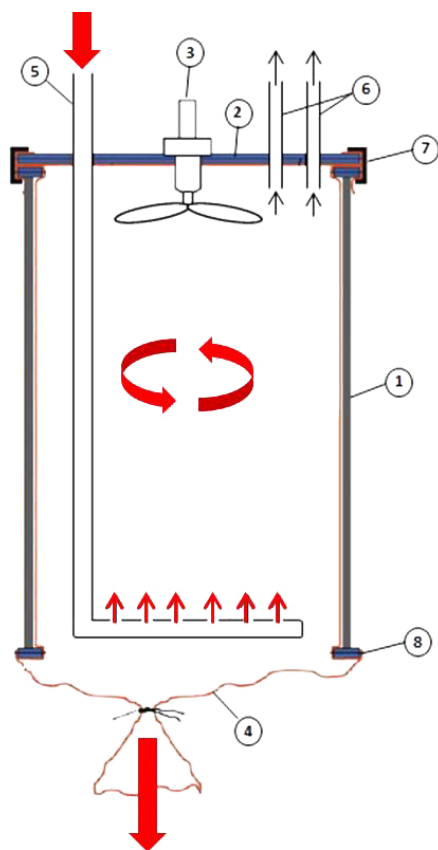
Figure 2. Layout of the dynamic cuvette as used in this study. 1 – PVC frame; 2 – acrylic glass cap; 3 – fan coated with Teflon; 4 – FEP foil; 5 – inlet PFA-tube with additional ring; 6 – sample tubes; 7 – clamps; – 8 silicon strip.

rated ring at the bottom of the cuvette the main air stream was divided into several small air streams to improve the distribution of the air addition inside the cuvette. Air samples were withdrawn by the two sampling tubes entering the cuvettes from the top. The surplus of the air stream effused at the vent situated at the bottom of the cuvette (see Fig. 2). To prevent ambient air from entering the cuvette, the flow rates were adjusted such that the cuvettes were slightly over-pressurized. For an accurate performance of the dynamic cuvettes potential deposition of the trace gases on the cuvette walls and the influence of chemical gas phase reactions have to be known and quantified. The deposition rate $k_{\text{dep,wall}}$ represents the amount of molecules which deposit on the foil surface of the cuvette per time and is defined according to Bonn et al. (2013) as Eq. (1):

$$k_{\text{dep,wall}} = \ln\left(\frac{\text{vmr}_{\text{in, trace gas}}}{\text{vmr}_{\text{out, trace gas}}}\right) \times \frac{1}{\tau}, \qquad (1)$$

where $\text{vmr}_{\text{in, trace gas}}$ is the initial mixing ratio, $\text{vmr}_{\text{out, trace gas}}$ is the outlet mixing ratio of the trace gas species, respectively, and τ the residence time of air in the dynamic cuvette. Under well-mixed conditions, τ of air within the dynamic cuvette is

determined as the ratio between the cuvette volume V_{cuvette} and purging rate f_{purg}:

$$\tau = \frac{V_{\text{cuvette}}}{f_{\text{purg}}}. \qquad (2)$$

The choice of the appropriate residence time in the cuvette is a key factor for the operation of a dynamic cuvette system. On the one hand, it should be short enough to exclude chemical reactions in the cuvette and to follow potential fast changes in the environment. In the case of PAN, the thermal decomposition under higher temperature made it necessary to keep the residence time inside both cuvettes as short as possible. As the lifetime of PAN was about 5 hours at the cuvette temperature of 25 °C (calculated from the rate coefficient suggested by Atkinson et al., 2006) the thermal decomposition of PAN did not affect the uptake measurements by the leaves. On the other hand, the residence time has to be low enough to receive a sufficient mixing ratio difference caused by the enclosed leaf material that can be resolved by the analytical system. For a dynamic cuvette with well-mixed flow conditions, the residence time is equal to the flushing time as defined in Eq. (2). With a cuvette volume of 70 L and an operating air flow of about 20 L min^{-1} for each cuvette the residence time inside the cuvette was 3.4 min.

2.1.3 Automatic temperature regulated air humidification system (ATRAHS)

We present an automatic temperature regulated air humidification system (ATRAHS) to control the relative humidity inside the cuvettes. Due to the high operating main flow rate of 20 L min^{-1} and the resulting short residence time of the dry air stream inside the humidifier tank for each cuvette, we chose to humidify the main dry air stream directly with the challenge to obtain a high humidification efficiency. ATRAHS consists of two stainless steel tanks (humidifier tank), one for each cuvette, with a tank volume of 1.5 L (see Fig. 3). The tanks were filled with deionized water and heated by a heat element. The dry air stream was purged through the head space of the tank and was thereby humidified due to the high vapor pressure of heated water. An additional tank served as a water reservoir, which was connected to a deionized water supply. The water level in this tank was regulated by a floating valve. Due to the hydrostatic pressure of the water inside the storage tank, the humidifier tank was kept on a constant level automatically. With this setup, the humidifier provided an unlimited water reservoir for the humidification procedure at a constant ratio of water level to headspace. Therefore, at a given air flow rate the resulting humidity depended mainly on the water temperature, which was controlled by an electronic control device (V25) developed by the MPIC electronic workshop. The temperature and relative humidity before and inside the cuvettes were determined by two sensors for each dynamic cuvette (Hygromer® MP 100 A, Rotronic Messgeräte GmbH, Germany). A routine was
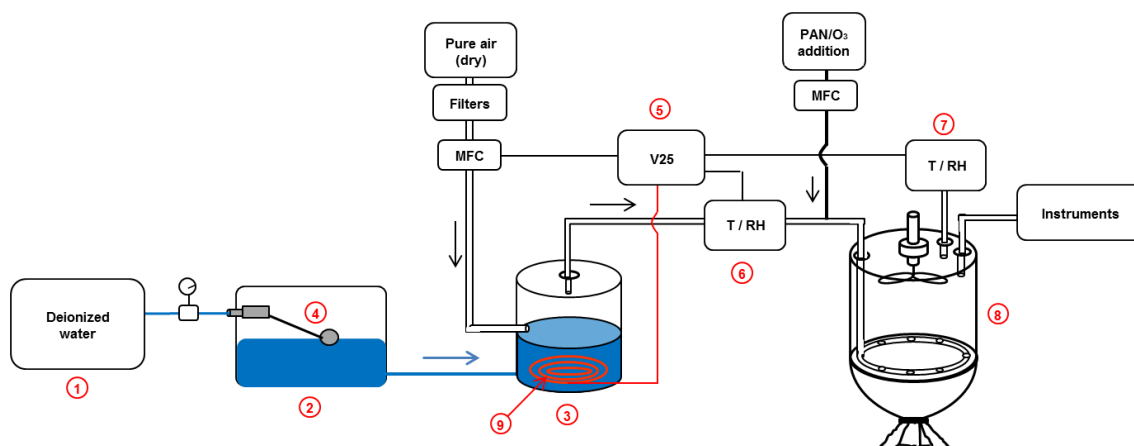
Figure 3. Flow chart of the automatic temperature regulated air humidification system (ATRAHS). 1 – deionized water supply; 2 – water storage tank; 3 – humidifier tank; 4 – float valve; 5 – V25 control device; 6 – T/RH sensor (initial regulation); 7 – T/RH sensor (monitoring); 8 – dynamic cuvette; 9 – heat element.

developed to regulate the heating temperature automatically to obtain a constant humidity value inside the cuvettes. The initial humidity of the air stream measured by the humidity sensor in front of the cuvette (see Fig. 3, No. 6) was used for the humidity regulation with V25. The humidity sensor behind the cuvette (see Fig. 3, No. 7) was needed to monitor the adjusted humidity value inside the cuvette. To avoid the O_3 or PAN from coming into contact with the stainless steel and water surface, the gas addition system was installed after the humidifier tank. For testing the humidification system, the relative humidity inside both cuvettes (RH_{cuv}) was manipulated in an additional experiment adjusting an initial humidity (RH_{in}) level from 50 to 100 % for both cuvettes over a time period of 75 h including light and dark periods (see Sect. 3.1.2).

2.1.4 Leaf wetness sensor

The leaf wetness sensors were used to identify and characterize the formation of liquid water films on the leaf surface. The technique is based on the measurement of the electrical resistance of the surface between two electrodes, which are fixed on the leaf with metal clamps (see Fig. 4). The sensor design is based on that published by Burkhardt and Ei-den (1994), and has been updated according to suggestions of J. Gerchau (2011, personal communication). Briefly, an oscillator generates an alternating voltage (2 VAC) with an adjustable frequency between 0.5 and 2 kHz. This voltage is applied to the leaf surface, which acts as a resistor in a volt-age divider circuit. The resistance of the leaf surface, which is derived directly from the resistive voltage drop, depends on the leaf surface wetness. A major drawback of the old sensor design was the temperature dependence of the signal (e.g., Altimir et al., 2006) caused by changing resistance of the cable between the leaf clamp and the measuring device. This has now been solved by using a miniaturized sensor
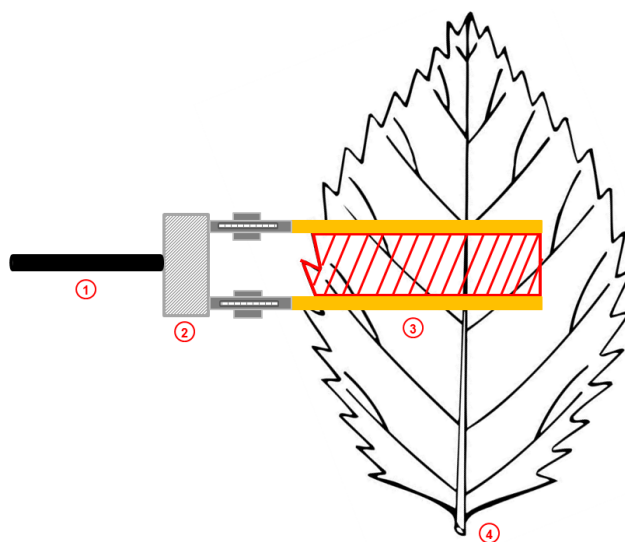
Figure 4. Draft of the leaf wetness sensor. 1 – data cable; 2 – sensor; 3 – electrode clams; 4 – plant leaf. Modified from Burkhardt and Gerchau (1994).

board measuring the leaf resistance with a voltage divider circuit including a capacitor and a pre-amplifier directly at the clamps of the sensor (see Fig. 4). Additionally, the oscillator can be tuned to four different frequencies from 0.5 to 2 kHz, which allows conductivity measurements also at high ionic strengths (activities), i.e., at low ion mobility. Furthermore, all sensors are now evaluated independently with individual sensor boards as well as individual amplifier and rectifier circuits before A/D conversion in order to avoid interferences between different leaf measurements. In this study, we present measurements of the optimized version of the leaf wetness sensor. For the sample cuvette, three sensors were mounted on plant leaves at different heights to obtain an av-

erage value, which was regarded as representative for the entire plant. The background signals were measured by sensors without leaves in the reference cuvette. The net-signals were used to calculate the electrical surface conductance G in μS, Eq. (3).

$$G = 1019 \times U^{-1.062}, \tag{3}$$

where G (μS) is the electrical surface conductance and U (mV) is the measured voltage raw signal by the sensor.

2.2 Test experiment with O_3 and PAN

A long-term flux measurement was performed over a period of 14 days to demonstrate the quality of the twin-cuvette setup.

2.2.1 Plant material and growth conditions

The experiments were performed with 3-year-old tree individuals of *Quercus Ilex* (ordered from Burncoose & South Down Nursery, Gwennap, Redruth, Cornwall, UK), a plant species typical for the Mediterranean region. After delivery, the trees grew up in pots with commercial soil mixture (FloraSelf, Germany) in the institute's own greenhouse under natural growing conditions ($T_{winter} = 15\,°C$, $T_{summer} = 30\,°C$, $PAR_{max} = 1400\,\mu mol\,m^{-2}\,s^{-1}$). The plants were watered daily in the summer period and in the winter period every 3 days. Measurements started after four days of acclimatization of the sample plant inside the cuvette. Measurements were performed with two replicates of the plant species.

2.2.2 Plant cabinet conditions

The diurnal cycle of the plant was simulated by the plant cabinet system with 13 h of light and 11 h of dark period. The light intensity (450–650 nm) was kept constant at $600\,\mu mol\,m^{-2}\,s^{-1}$ for all day light conditions by eight HQI®-BT lamps (400 W, OSRAM GmbH, Germany) and six Krypton lamps (100 W, General Electric Company, USA). The cabinet temperature was held constant during the light period at $T = 28 \pm 0.1\,°C$ and at dark period at $23 \pm 0.1\,°C$.

2.2.3 Determination of the leaf area

For a non-destructive determination of the leaf area the shape of every single leaf of the sample plant was drafted by hand and digitalized via a photo scanner (Epson Perfection 3170 Photo). The scans were evaluated by the program "Compu eye, Leaf & Symptom Area" (Bakr, 2005) to obtain the overall leaf area.

2.2.4 Application of abscisic acid

Abscisic acid (ABA) is a plant hormone, which affects the closure of the leaf stomata. For the experiments, a branch was cut from the plant under water to prevent embolism. The

stock solution of ABA was created by dissolving solid ABA (CAS 14375-45-2, Sigma Aldrich, USA) in 5 mL ethanol and then filling up to 100 mL with deionized water. The nutrient solution was concentrated with 250 μM ABA for the O_3 experiment and 350 μM for the PAN experiment. For the fumigation of the plant, 60 ppb O_3 and 310 ppt PAN were used. Additionally, the nutrient solution contained 1 mM of potassium chloride (KCl), 0.1 mM of sodium chloride (NaCl) and 0.1 mM of calcium chloride (CaCl$_2$) (Chaparro-Suarez et al., 2011). For the ABA experiments, the branch was introduced to the cuvette for 3 days for acclimatization before the measurement started.

2.2.5 Calculation of fluxes and plant exchange parameters

As we could assume constant conditions in the cuvettes over the time of 10 min switching intervals, the mixing ratios of all four measured positions (inlet and outlet of both cuvettes) could be used to derive the deposition fluxes of O_3 and PAN. The fluxes were determined from the differences of trace gas mixing ratios of the reference and sample cuvettes as follows (see e.g., Teklemariam and Sparks, 2004), Eq. (4):

$$F\,(O_3, PAN) = -\frac{f_m \times (vmr_{out,ref} - vmr_{out,sample})}{A_{leaf}}, \tag{4}$$

where F is the flux of O_3 ($nmol\,m^{-2}\,s^{-1}$) and PAN ($pmol\,m^{-2}\,s^{-1}$), respectively. f_m ($mol\,s^{-1}$) is the mole flow rate through each cuvette, which is calculated from the volume flow rate f_v ($L\,s^{-1}$) divided by $24.4\,L\,mol^{-1}$ (at 25 °C and 1013.25 hpa), i.e., the volume of one mole in air at standard conditions, which can be used as the conditions in the set cabinet were close to standard conditions (see Sect. 2.2.2). A_{leaf} (m^2) is the leaf area of the entire plant inside the sample cuvette. $vmr_{out,ref} - vmr_{out,sample}$ is the difference of the trace gas mixing ratio between the reference and sample cuvette. The same equation was used to calculate the water flux E ($mmol\,m^{-2}\,s^{-1}$) with the mixing ratio difference of the water vapor between both cuvettes.

The deposition velocity V_d ($mm\,s^{-1}$) of O_3 and PAN was calculated following Eq. (5):

$$V_d\,(O_3, PAN) = \frac{F\,(O_3, PAN)}{vmr_{out,sample}} \times V_m, \tag{5}$$

where V_m is the molar volume of $22.4\,L\,mol^{-1}$ at 25 °C.

The stomatal conductance is an important parameter to evaluate the gaseous uptake from the ambient air into the plant leaves. The stomatal conductance of water vapor $g_{s,calc}(H_2O)$ ($mmol\,m^{-2}\,s^{-1}$), Eq. (6) was determined from the ratio between the water flux E ($mmol\,m^{-2}\,s^{-1}$) and the air-to-leaf-vapor-pressure deficit VPD ($Pa\,kPa^{-1}$):

$$g_{s,calc}(H_2O) = \frac{E}{VPD}, \tag{6}$$

where VPD is given according to von Caemmerer and Farquhar (1981) as Eq. (7):

$$VPD = \frac{SVP(T_{leaf})}{P_{sample}} - C_{out,sample}(H_2O). \quad (7)$$

The saturation water vapor pressure SVP (hPa) was calculated with the Goff–Gratch equation (Goff and Gratch, 1946), which is dependent on the leaf temperature T_{leaf}. P_{sample} (kPa) is the pressure in the sample cuvette and $C_{out,sample}$ (H_2O) ($Pa\,kPa^{-1}$) is the concentration of water vapor inside the sample cuvette. The stomatal conductances of O_3 and PAN were determined following Eq. (8) from the stomatal conductance to water vapor multiplied by the ratio of the diffusion coefficients of the respective trace gas (O_3, PAN) and H_2O:

$$g_{s,calc}(O_3, PAN) = g_{s,calc}(H_2O) \times \frac{D_{O_3,PAN}}{D_{H_2O}}. \quad (8)$$

The diffusion coefficients of O_3, PAN and H_2O are $D_{O_3} = 0.137\,cm^2\,s^{-1}$ (Laisk et al., 1989), $D_{PAN} = 0.089\,cm^2\,s^{-1}$ (Sparks et al., 2003) and $D_{H_2O} = 0.25\,cm^2\,s^{-1}$ (Marrero and Mason, 1972), respectively.

The internal leaf O_3 and PAN mixing ratios were determined according to Teklemariam and Sparks (2004) by following equation Eq. (9):

$$vmr_{int,leaf} = vmr_{out,sample} - \left(\frac{F(O_3, PAN)}{g_{s,calc}(O_3, PAN)} \right). \quad (9)$$

Measured leaf conductance $g_{s,meas}$ ($mmol\,m^{-2}\,s^{-1}$) to O_3 and PAN was calculated according to the equation scheme of Teklemariam and Sparks (2004), Eq. (10):

$$g_{s,meas}(O_3, PAN) = \frac{F(O_3, PAN)}{vmr_{out,sample} - vmr_{int,leaf}}. \quad (10)$$

For O_3 and PAN, $vmr_{int,leaf}$ is assumed to be closed to zero (Laisk et al., 1989).

2.3   System characterization and quality assurance

2.3.1   Evaluation of the twin-cuvette system and O_3 and PAN loss

As mentioned above, the advantage of a twin-cuvette setup was to account for disturbing background effects such as wall deposition, assuming that these effects were equal for both cuvettes. In order to check the accuracy and stability, the mixing ratio measurements of O_3 and PAN were compared when both cuvettes were empty. Inside an empty cuvette, the inner mixing ratio was defined as difference between the inlet

and outlet of the cuvette, Eqs. (11) and (12):

$$vmr_{ref,diff} = vmr_{ref,in} - vmr_{ref,out} \quad (11)$$

$$vmr_{sample,diff} = vmr_{sample,in} - vmr_{sample,out}. \quad (12)$$

The mixing ratio difference between both cuvettes was defined as follows, Eq. (13):

$$vmr_{diff} = vmr_{sample,diff} - vmr_{ref,diff}. \quad (13)$$

By combination of Eqs. (11)–(13) we received Eq. (14):

$$vmr_{diff} = vmr_{ref,out} - vmr_{sample,out} + vmr_{sample,in} - vmr_{ref,in}. \quad (14)$$

Given that the inlet mixing ratios between both cuvettes are identical ($vmr_{diff,in} = vmr_{sample,in} - vmr_{ref,in} = 0$), the mixing ratio difference between both cuvettes could be simplified as Eq. (15):

$$vmr_{diff,out} = vmr_{ref,out} - vmr_{sample,out}. \quad (15)$$

The described evaluation experiment was conducted over 8 hours at which the inlet O_3 and PAN mixing ratios were held constant at 59.5 ppb and 324 ppt, respectively.

In addition to accounting for effects in the cuvettes, the O_3 and PAN mixing ratios were determined systematically with and without the cuvettes as well as at different positions of the setup to quantify the losses of both gas species on the material surface as tubes, addition pump, cuvette foil and valve block.

2.3.2   Calibration procedure

Calibration of the O_3 analyzer and PAN GC-ECD were performed at all inlet and outlet positions of the dual cuvette system using multiple O_3 and PAN mixing ratios (9, 18, 37, 74, 86 ppb and 195, 380, 656, 896 ppt, respectively) (see Fig. 7). The O_3 analyzer was calibrated with a GPT (gas phase titration calibrator, Sonimix 6000C2, LN Industries, Switzerland) in combination with a NO_x analyzer (49i, Thermo Fisher Scientific, USA). A NO standard gas 10 ± 0.33 ppm was used to calibrate the NO_x analyzer. The determination of the set O_3 mixing ratio occurred from the titration of the diluent NO mixing ratio by a certain O_3 level produced with an internal UV lamp of the GPT. The calibration of the PAN GC-ECD was performed via a PAN calibration unit. A mixture of NO standard gas (2 ± 0.04 ppm) and synthetic air stream is enriched with acetone in a permeation cell. PAN is then produced by photolysis of acetone an internal UV lamp in presence of NO and O_2 (Patz et al., 2002). The detection limit (LOD) of the O_3 analyzer and PAN GC-ECD was determined as 3σ of the zero noise level. As the ECD showed a temperature dependency, the entire PAN GC-ECD was placed inside an additional climate cabinet to keep the ambient temperature constant at 23 °C.

2.3.3 Random flux error calculation and statistical significance

The precision of the O_3 analyzer and the GC-ECD was determined by supplying constant initial O_3 and PAN mixing ratios (59.5 ppb and 324 ppt) and measuring them consecutively at both the inlet and outlet positions of both dynamic cuvettes for 8 h. Determining the precision via the inlet and outlet positions instead of just determining the precision of the gas analyzers itself, ensured to obtain precision values which are representative for the actual measurements of mixing ratio differences required for the flux calculation. The relative precision at each position was determined in Eq. (16) by the standard deviation (1σ) divided by the mean value.

$$\text{precision}[\%] = \frac{\text{standard deviation}(\text{vmr}_{O_3,PAN})}{\text{mean value}(\text{vmr}_{O_3,PAN})} \times 100 \quad (16)$$

The random errors of F, $g_{s,calc}$, $g_{s,meas}$ and V_d were calculated using general representation of the Gaussian error propagation (Bevington and Robinson, 2003), Eq. (17):

$$u(x_{i,j}) = \quad (17)$$
$$\sqrt{\sum_{i=1}\left(\frac{\partial u}{\partial x_i}\right)^2 \times (\Delta x_i)^2 + \sum_{i=1}\sum_{j=1}\left(\left(\frac{\partial u}{\partial x_i}\right)\left(\frac{\partial u}{\partial x_j}\right)\Delta x_i \Delta x_j r(x_i, x_j)\right)}$$
$$i \neq j.$$

Δu is the random error of the respective parameter (i.e., F, g_s and V_d), which can be expressed as a function of n individual quantities ($x_{i,j}$). $\partial u/\partial x_{i,j}$ are the partial derivatives of the function. Δx_i and Δx_j are the random error of the error-prone variables. $r(\Delta x_i, \Delta x_j)$ is the correlation coefficient between two dependent variables x_i and x_j. In the case that the variables are uncorrelated, the term $\Delta x_i \Delta x_j r(x_i, x_j)$ is zero.

The significance of the mixing ratio difference between each sampling position of the reference and sample cuvette was proved with an independent two-sample-t-test, using a α-significance level of 0.05. The Pearson correlation coefficient R_{pearson} with 95 % confidence interval was calculated with the statistic software described in Mudelsee (2003).

3 Results

3.1 Performance of the twin-cuvette system

3.1.1 Quality of O_3 and PAN measurements

Comparison between the empty sample and reference cuvettes

The comparison of both empty cuvettes (see Sect. 2.3.1) showed only insignificant differences (i.e., $p > 0.05$ in the t test) in O_3, PAN and CO_2 mixing ratio between both inlet and outlet sampling positions of the cuvettes. As mentioned in Sect. 2.3.1, the O_3 and PAN initial mixing ratios
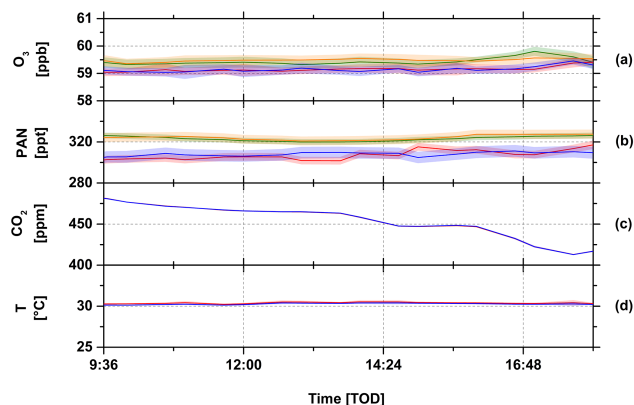
Figure 5. Comparison of the all key parameters between both empty cuvettes to indicate their identity. **(a)** O_3 mixing ratio, **(b)** PAN mixing ratio, **(c)** CO_2 mixing ratio, green line: inlet position of the reference cuvette; orange line: inlet position of the sample cuvette; red line: outlet position of the reference cuvette; blue line: outlet position of the sample cuvette; **(d)** cuvette inner temperature, reference cuvette (red) and sample cuvette (blue). The colored area represents the uncertainty of the calculated mean values over an average time period of 10 min.

Table 2. Minimal resoluble mixing ratio difference of O_3 and PAN between both cuvettes.

Sampling positions	$\text{vmr}_{\text{diff},O_3}$ (ppb)	$\text{vmr}_{\text{diff},PAN}$ (ppt)
Inlet	0.05 ± 0.35	1.29 ± 7.16
Outlet	0.01 ± 0.33	0.68 ± 9.35

were held constant with 59.4 ppb in O_3 and 324 ppt in PAN over a time period of 8 hours (see Fig. 5). For O_3 $\text{vmr}_{\text{diff,in}}$ was 0.05 ± 0.35 ppb and $\text{vmr}_{\text{diff,out}}$ was 0.01 ± 0.33 ppb. For PAN $\text{vmr}_{\text{diff,in}}$ was 1.29 ± 7.16 ppt and $\text{vmr}_{\text{diff,out}}$ was 0.68 ± 9.35 ppt (see Table 2). Over the duration of the experiment, the CO_2 mixing ratio declined steadily from 480 to 400 ppm, which was due to the fact that ambient CO_2 was not retained by the air purification. The magnitude of the variation in the CO_2 mixing ratio is considered as not large enough to have a significant effect on the plant metabolism and thus on the uptake of O_3 and PAN. Temperature differences between the cuvettes were also insignificant, although the temperature in the climate cabinet was 5 K less during dark than during light periods (data not shown).

Precision and detection limit (LOD) of the cuvette system

To include the potential influence of cuvette system on the LOD and the precision of the O_3 and PAN measurements, the calibrations were also performed at different sampling positions of the cuvette system (Table 3). The calibration curves of both analyzers were linear with a slope of 3.3×10^{-2} ($R^2 = 0.99$) for the ozone analyzer and 164.2 ($R^2 = 0.99$)

Table 3. Detection limit (LOD) and precision of the twin-cuvette system at different sampling positions. The determination of the LOD is based on 3σ of the blank value.

Trace gas	Sampling position	LOD (3σ)	adjusted mixing ratio	Precision (%)
O_3	Inlet sample	0.8 ppb	59.4 ppb	0.3
	Inlet reference	0.9 ppb	59.4 ppb	0.3
	Outlet sample	0.9 ppb	58.8 ppb	0.3
	Outlet reference	0.9 ppb	58.8 ppb	0.3
PAN	Inlet sample	1 ppt	324.4 ppt	1.4
	Inlet reference	1 ppt	323.1 ppt	1.1
	Outlet sample	1.2 ppt	307.6 ppt	1.8
	Outlet reference	1.3 ppt	306.6 ppt	1.2

for the PAN GC-ECD (see Fig. 7). While a small loss of O_3 and PAN can be observed in the experiments (see Sect. 3.1.3 for detailed analysis of potential losses within the cuvette system), the LOD ranged for O_3 between 0.8 and 0.9 ppb and for PAN between 1 and 1.3 ppt. The precision for O_3 was 0.3 % and for PAN between 1.4 and 1.8 %.

### 3.1.2   Quality of the humidity regulation with ATRAHS

The initial humidity (RH_{in}) controlled by ATRAHS was very constant. When increasing the set humidity value gradually from 50 to 90 %, the relative humidity became constant within several minutes after each change (see Fig. 6). RH_{cuv} was 9 % lower than RH_{in} during the dark period and 12 % lower during the light period, which is caused by the addition of dry air from the O_3 and PAN addition downstream of the RH_{in} humidity probe. The difference of 3 % RH_{cuv} between light and dark period was caused to the inner cuvette temperature, which is 3 °C higher than the environmental temperature of the plant cabinet during the light period. In the dark period, both inner temperatures were the same. There was no significant difference of RH_{cuv} observed between both cuvettes up to a value of 70 % in the light and 80 % in the dark period. Above those values, RH_{cuv} fluctuated strongly, which could be the cause of water condensation inside the cuvettes. The condensation at 80 % RH_{cuv} did not occur during the dark period, presumably as the temperature difference between the cuvettes and the plant cabinet environment was close to zero, which also explains the adjusting of higher RH_{cuv} values up to 90 % in the dark period. Furthermore, the heating temperature (T_{heater}) of both humidifiers was higher during the light periods, caused by its regulation, which vaporized more water to compensate for the lower relative humidity. Beyond 90 % RH_{in} in the light, the heating temperature began to decrease continuously, which was as a result of decreasing water demand due to the water condensation.
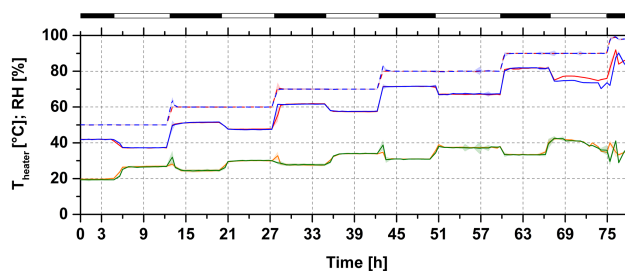

Figure 6. Relative humidity controlled by ATRAHS at different levels from 50 to 100 %. Straight red line: RH_{cuv} of the reference cuvette; straight blue line: RH_{cuv} of the sample cuvette; dotted red line: RH_{in} of the reference cuvette; dotted blue line: RH_{in} of the sample cuvette; orange line: T_{heater} of the reference humidifier; green line: T_{heater} of the sample humidifier. The diurnal cycle of light was simulated by a climate cabinet with 6 h light period (white balk) and 6 h dark period (black balk).

3.1.3   Loss of O_3 and PAN within the system

For both, O_3 and PAN, the calibrations with inclusion of the total setup performed by sampling at different positions of the cuvette setup exhibited a weaker slope than calibrating the analyzers without setup. This indicates a loss of O_3 and PAN inside the setup, caused by tubing, connectors, MFCs, valves, pumps and the cuvette itself (see Fig. 7). The overall loss measured at the different sampling positions was 18.2 % in O_3 and 16.3 % in PAN mixing ratios. For O_3, the difference between the inlet and outlet positions was not significant, indicating the major O_3 loss not to be caused by the cuvettes themselves. For PAN, a 5 % difference between the cuvette inlet and outlet was found, which is most likely associated with deposition of PAN to the foil surface (see also Sect. 3.1.1, Fig. 5). The O_3 and PAN losses were nearly identical for both the sample and reference cuvettes, confirming the identical behavior of the twin-cuvette system. To determine the loss of O_3 and PAN, which was not attributed to the cuvettes, the O_3 and PAN mixing ratios were measured downstream of the Teflon membrane pump, the MFCs, the cuvettes and the Teflon valves (listed in order of appearance in the flow path, see Fig. 1). As shown in Fig. 8, different slopes of the calibration curves were observed depending on the sampling location, indicating an increase of the O_3 and PAN losses in some parts of the cuvette/piping system. For example, a loss of O_3 of 6 % and a loss of PAN of 9.5 % was induced by the Teflon pump. As the air inside the Teflon pump heated up to 50 °C, thermal decomposition of PAN could have contributed to the higher loss of PAN. However, as the lifetime of PAN was about 10 min for these conditions and the residence time of the gas stream inside the Teflon pump tube was calculated as 3.5×10^{-2} s, a significant contribution of thermal decomposition to the PAN loss at the Teflon pump can be excluded. For O_3, the highest loss of 9.7 % occurred while the gas stream passed through
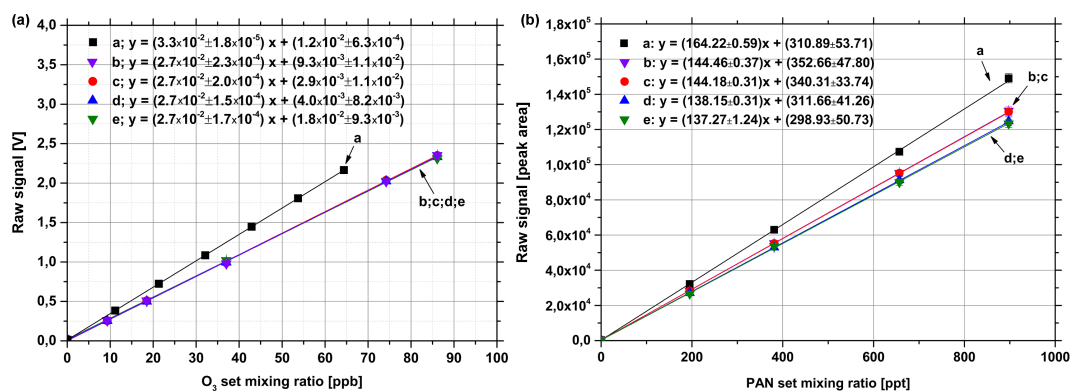
Figure 7. Multipoint calibration curve of O_3 (left) and PAN (right) at different sampling positions: **(a)** without setup, **(b)** inlet of the sample cuvette, **(c)** inlet of the reference cuvette, **(d)** outlet of the sample cuvette, **(e)** outlet of the reference cuvette. The linear fit equations are given with the error of slope and offset.
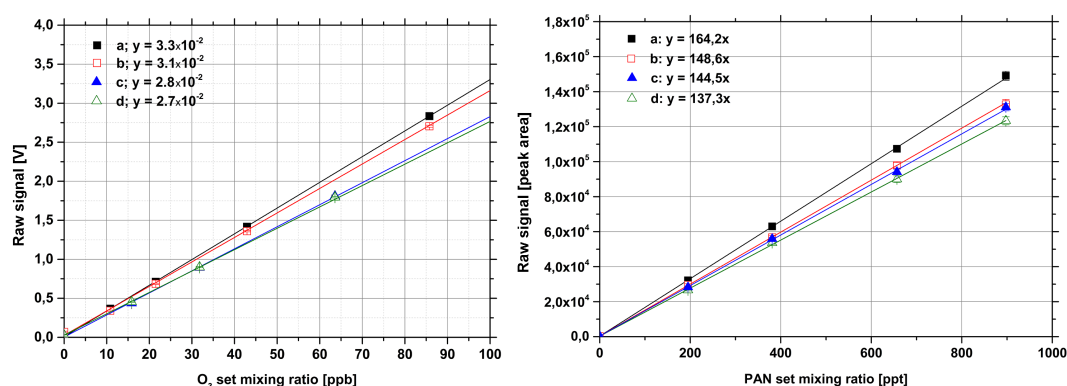
Figure 8. Systematical determination of the O_3 and PAN loss at different locations of the cuvette setup. **(a)** analyzer directly connect with calibration unit without setup, **(b)** including teflon pump, **(c)** including MFCs for gas addition, **(d)** including cuvettes and valve block system.

the MFCs. This O_3 loss is most likely caused by the reaction of O_3 with the inner surface of the MFC, which was made of stainless steel. Furthermore, the MFCs had an operational temperature of nearly 30 °C, which could promote the loss process. The O_3 loss between the inlet position and outlet of the dynamic cuvette including the Teflon valve block system was less reaching 3.5 %. For PAN the loss within the cuvette was only slightly higher than for O_3 reaching 5 %. The wall deposition rate $k_{\mathrm{dep,wall}}$ for PAN was found to range around $(2.55 \pm 0.78) \times 10^{-4}\,\mathrm{s}^{-1}$ in the reference cuvette and $(2.54 \pm 0.44) \times 10^{-4}\,\mathrm{s}^{-1}$ in the sample cuvette (Table 4). In case of O_3, $k_{\mathrm{dep,wall}}$ was $(2.78 \pm 0.63) \times 10^{-5}\,\mathrm{s}^{-1}$ in the reference cuvette and $(2.76 \pm 0.64) \times 10^{-5}\,\mathrm{s}^{-1}$ in the sample cuvette (data for the calculation of $k_{\mathrm{dep,wall}}$ see Fig. 5). The finding that the wall deposition rates for both gases were not significantly different comparing both cuvettes was supporting the use of a twin-cuvette system with an identical construction. The fact that $k_{\mathrm{dep,wall,PAN}}$ exceeded $k_{\mathrm{dep,wall,O_3}}$ by 1 order of magnitude shows the significantly higher wall deposition of PAN than O_3. Due to the short residence time of 3.4 min and a life time of PAN inside the cuvette of 5 h

**Table 4.** Wall deposition rate of O_3 and PAN within the dynamic cuvettes.

Dynamic cuvettes	$k_{\mathrm{dep,wall}}$PAN (s^{-1})	$k_{\mathrm{dep,wall}}$O$_3$ (s^{-1})
Reference	$(2.55 \pm 0.78) \times 10^{-4}$	$(2.78 \pm 0.63) \times 10^{-5}$
Sample	$(2.54 \pm 0.44) \times 10^{-4}$	$(2.76 \pm 0.64) \times 10^{-5}$

(see Sect. 2.1.2) thermal decomposition of PAN could be excluded as a reason for the higher deposition of PAN.

3.2 Flux measurements under laboratory conditions

3.2.1 Test run and flux rates

The twin-cuvette system could be successfully adapted to the needs of the plants and the experimental conditions needed. Measurements were performed under a light/dark cycle with a maximum of 480 µmol photons m^{-2} s^{-1} in the light period (see Fig. 9a). Leaf temperature (T_{leaf}) rose to 27 °C in the
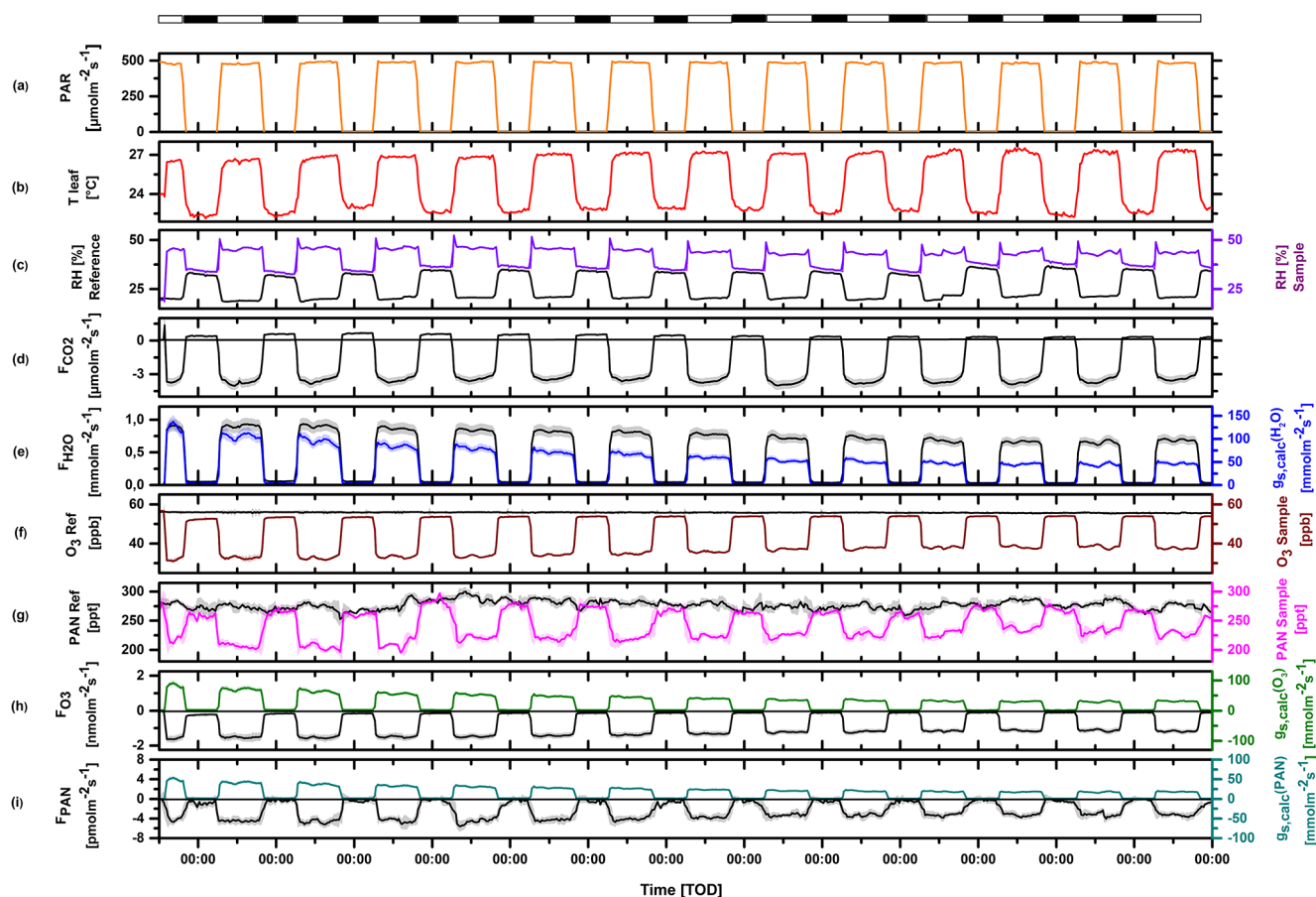
Figure 9. Long-term flux measurement of *Quercus Ilex* at constant initial mixing ratio ($O_3 = 57$ ppb, $PAN = 280$ ppt) over 14 days. **(a)** light density, **(b)** leaf temperature, **(c)** relative humidity of the reference (black) and sample (violet) cuvette, **(d)** CO_2 exchange flux, **(e)** transpiration rate (black) and stomatal conductance to water vapor (blue), **(f)** O_3 mixing ratio of the reference cuvette (black) and sample cuvette (brown), **(g)** PAN mixing ratio of the reference cuvette (black) and sample cuvette (magenta), **(h)** O_3 exchange flux (black) and O_3 conductance (green), **(i)** PAN exchange flux (black) and PAN conductance (dark cyan). The diurnal cycle of light was simulated by a climate cabinet with 13 h light period (white balk) and 11 h dark period (black balk). The inner area of the cabinet had a temperature of 25 °C and relative humidity of 50 %.

light period and decreased in the dark period to 22 °C (see Fig. 9b). The relative humidity in the reference cuvette represented the background value with a minimum of 22 % during the dark periods and a maximum of 37 % at light periods (see Fig. 9c).

The relative humidity in the sample cuvette was significantly enhanced by the transpiration of the plant. During the dark periods the relative humidity of the sample cuvette was 38 %, a similar value as compared to the reference cuvette when the leaf stomata were closed and plant transpiration was inhibited. During the light periods, the humidity level inside the sample cuvette reached 47 %. The water transpiration and CO_2 exchange of the plant showed a typical behavior related to the light and dark periods. The CO_2 flux had a minimum of $-3 \, \mu mol \, m^{-2} \, s^{-1}$ and a maximum of $0.8 \, \mu mol \, m^{-2} \, s^{-1}$, which represents a CO_2 uptake under light and an emission under dark conditions (see Fig. 9d).

The water flux showed a maximum of $0.9 \, mmol \, m^{-2} \, s^{-1}$ during light periods. At dark periods it was close to zero (see Fig. 9e). There was a slight decreasing trend of water flux over the measurement period, while after 10 days the water flux seemed to become constant. As expected, the stomatal conductance to water vapor $g_{s,calc}(H_2O)$ followed the same trend as the water flux (see also Fig. 9e). The mixing ratio of O_3 in the reference cuvette was constant at 55.8 ± 0.2 ppb (see Fig. 9f). In the sample cuvette the O_3 mixing ratio followed the plant diurnal cycle with a minimum of 32 ppb during the light period and a maximum of 55 ppb during the dark period, which was close to the reference value as the leaf stomata were closed due to the absence of light. The PAN mixing ratio in the reference cuvette was on average 277 ± 5 ppt during the measurement (see Fig. 9g). The mixing ratio in the sample cuvette followed the plant diurnal cycle similarly as O_3 with a minimum of 200 ppt during light periods and

Table 5. Comparison of the deposition velocity ratio of O_3 and PAN in previous studies.

Location	Method	Plant species	V_dPAN/V_dO$_3$	Reference
Laboratory	Climate chamber	*Medicago sativa*	0.37	Hill (1971)
	Wind tunnel setup	*Grass*	0.42	Garland and Penkett (1976)
	Twin-cuvette system	*Quercus ilex*	0.45 ± 0.04	This study
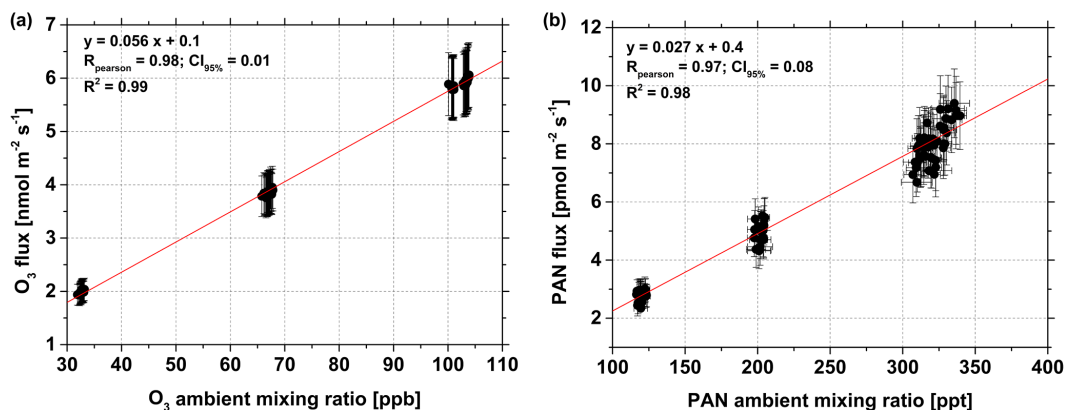
Figure 10. Behavior of O_3 and PAN flux with rising ambient mixing ratio. Both experiments were performed separately.

280 ppt during dark periods. The latter value is close to the reference PAN mixing ratio considering the precision of the PAN measurements (Table 3). The larger scatter in the results for PAN compared to O_3 are explained by the lower temporal resolution of the trace gas analysis. The O_3 and PAN exchange fluxes showed a clear diurnal trend with a maximum of $-1.6\,\mathrm{nmol\,m^{-2}\,s^{-1}}$ in O_3 and $-4\,\mathrm{pmol\,m^{-2}\,s^{-1}}$ in PAN under light conditions (see Fig. 9h and i, respectively). During dark periods, the minimum exchange flux for both species was close to zero, clearly indicating the role of stomatal control. Additionally, it should be noted that the fluxes during light conditions followed the same decreasing trend as the water flux and stomatal conductance for water vapor in the first 10 days of the experiment. During the light period, the calculated deposition velocity of O_3 (see Sect. 2.2.5) ranged from 0.66 to $1.06\,\mathrm{mm\,s^{-1}}$ and for PAN from 0.32 to $0.48\,\mathrm{mm\,s^{-1}}$. During the dark period, the deposition velocity was $0.05\,\mathrm{mm\,s^{-1}}$ for O_3 and close to $0\,\mathrm{mm\,s^{-1}}$ for PAN at $< 50\,\%$ RH. The ratio of the deposition velocity between O_3 and PAN was 0.45 ± 0.04 (Table 5). Compared with the only two existing literature values of previous studies, which were performed in the early 70s (Hill, 1971, Garland and Penkett, 1976), our deposition velocity ratio was close to Garland and Penkett (1976).

3.2.2 Correlation between ambient mixing ratio and uptake of O_3 and PAN

A clear linear relationship was found between the O_3 ($R_{\mathrm{pearson}} = 0.98$; $CI_{95\,\%} = 0.01$) and PAN ($R_{\mathrm{pearson}} = 0.97$; $CI_{95\,\%} = 0.08$) uptake by the leaf and the respective ambient

mixing ratios (see Fig. 10). By increasing the ambient ratio of O_3 from 32 to 105 ppb the exchange flux rose from 2 to $6\,\mathrm{nmol\,m^{-2}\,s^{-1}}$. In case of PAN the increase of the ambient mixing ratio from 100 to 350 ppt resulted in an increase of the PAN exchange flux from 2 to $10\,\mathrm{pmol\,m^{-2}\,s^{-1}}$. The ratio of the exchange fluxes of O_3 and PAN stayed constant at 0.48 ± 0.05 as derived from the ratio of the slopes. However, the observed deposition fluxes were about 50 % larger for similar O_3 and PAN mixing ratios as compared to the results shown in Fig. 9, which can be understood as a seasonal effect as the flux values shown in Fig. 10. This experiment was performed in June, instead of October of the same year.

3.2.3 Application of abscisic acid (ABA)

The ABA nutrient solution ($c = 250\,\mu M$) was added to the plant sample after 3 days of acclimatization. After adding the ABA, the measured O_3 mixing ratio in the sample cuvette rose from 72 to 87 ppb within a few hours (see Fig. 11a), which lead to a decrease of the O_3 deposition from -4.2 to $-0.4\,\mathrm{nmol\,m^{-2}\,s^{-1}}$ (see Fig. 11b) and a decrease of the stomatal conductance for O_3 from 63 to $5.5\,\mathrm{mmol\,m^{-2}\,s^{-1}}$ (see Fig. 11c). In the following light period, the O_3 mixing ratio as well as the O_3 flux persisted with the uncertainty at the same value as the reference. The stomatal conductance of O_3 was close to zero, which indicates an inhibition of the stomatal activity. After removing the ABA nutrient solution the O_3 mixing ratio in the sample cuvette decreased from 90 to 82.5 ppb within serval days. At the same time, the O_3 flux increased from -0.4 to $-1.8\,\mathrm{nmol\,m^{-2}\,s^{-1}}$, which was 42.8 % of the flux value before the plant was treated with
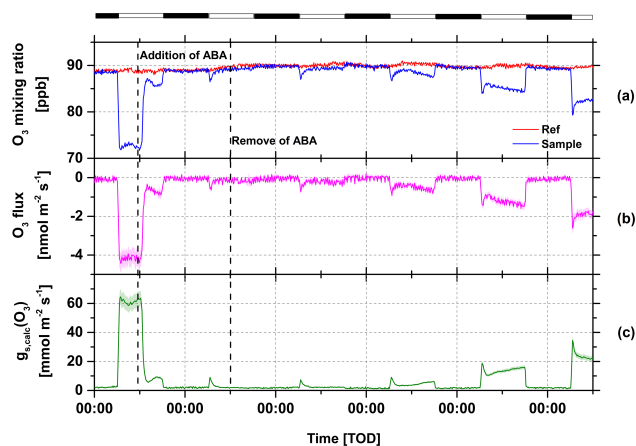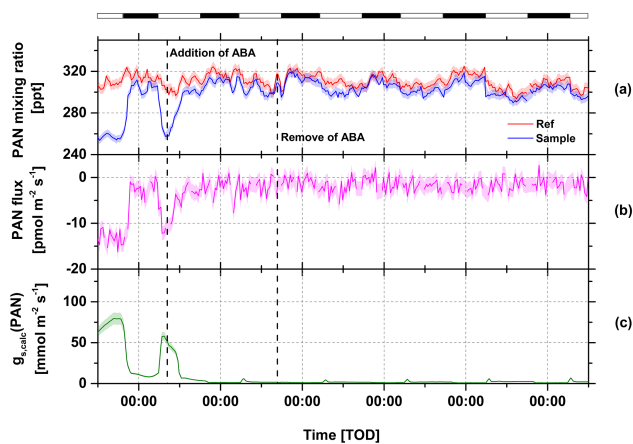
Figure 11. O_3 mixing ratio **(a)**, O_3 flux **(b)** and stomatal conductance to O_3 **(c)** measured at *Quercus ilex* treated with 250 μM ABA-nutrient solution. The diurnal cycle of light was simulated by a climate cabinet with 13 h light period (white balk) and 11 h dark period (black balk). RH inside both cuvettes was around 40 %.

Figure 12. PAN mixing ratio **(a)**, PAN flux **(b)** and stomatal conductance to PAN **(c)** for *Quercus ilex* treated with 350 μM ABA-nutrient solution. The diurnal cycle of light was simulated by a climate cabinet with 13 h light period (white area) and 11 h dark period (grey shaded area). RH inside both cuvettes was around 40 %.
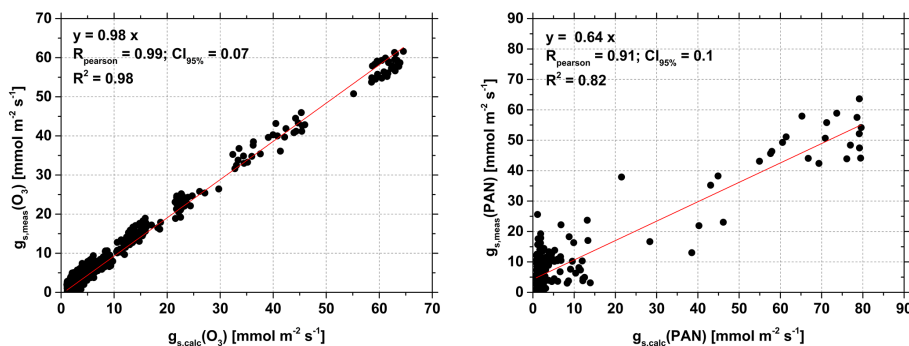
ABA. The stomatal conductance to O_3 increased from 2.2 to 23 mmol m^{-2} s^{-1}. The PAN experiment and the O_3 experiment (350 μM ABA nutrient solution) were performed separately (see Fig. 12). The PAN mixing ratio in the sample cuvette increased after the ABA addition from 258.4 to 301.4 ppt within a few hours (see Fig. 12a). The PAN deposition decreased from -12.1 to -1.1 pmol m^{-2} s^{-1} and then fluctuated between 0 and -4.8 pmol m^{-2} s^{-1} (see Fig. 12b). According to Table 2 the minimal resolvable deposition flux of PAN was -2.5 pmol m^{-2} s^{-1}. The stomatal conductance to PAN decreased from 57.9 to 6.8 mmol m^{-2} s^{-1} and was close to zero for the remaining time period (see Fig. 12c). Contrary to O_3, after removing the ABA nutrient solution, no significant change in the fluxes was observed. For O_3 and PAN, the measured stomatal conductance ($g_{s,meas}$) was plotted against the calculated stomatal conductance ($g_{s,calc}$) (see Sect. 2.2.5, Eq. 6) to investigate the partitioning between stomatal and non-stomatal deposition of O_3 and PAN on the plant leaves (see Fig. 13). A clear linear relationship between $g_{s,meas}$ and the $g_{s,calc}$ for O_3 ($R_{pearson} = 0.99$; CI$_{95\%} = 0.07$) and PAN ($R_{pearson} = 0.91$; CI$_{95\%} = 0.1$) was found with a slope of 0.98 ± 0.01 for O_3 and 0.64 ± 0.02 for PAN.

3.2.4 Influence of RH on electrical surface conductance

Of special interest is the question whether plant surfaces may act as a sink for trace gases without taking into account the stomatal deposition. Water soluble compounds can be affected significantly by water films on such surfaces (Burkhardt and Eiden, 1994). Our twin-cuvette system with the automatic temperature regulated humidification system (ATRAHS) can support experimental conditions to investigate such questions (see Fig. 6). As demonstrated, the electrical surface conductance G of the plant leaves rose with

the relative humidity in an exponential way ($R^2 = 0.96$) (see Fig. 14). The critical value of the relative humidity RH$_{crit}$, where G increases exponentially, was found at 60 % in this study. Above this value a formation of a liquid water film on the leaf surface was clearly observed.
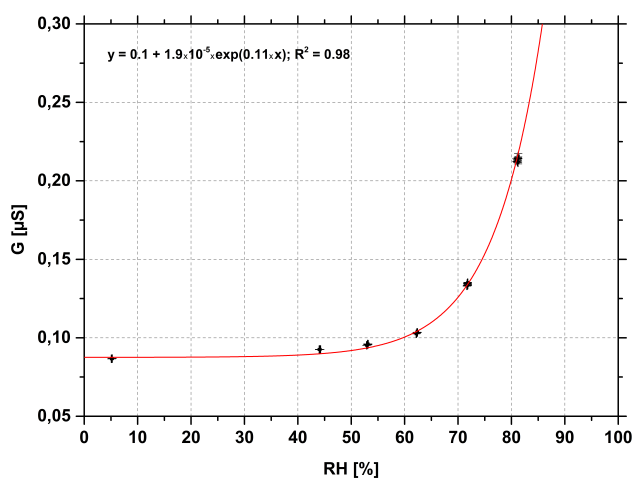
4 Discussion

4.1 Performance of the twin-cuvette system

4.1.1 Accuracy and consistency of O_3 and PAN measurements

With the presented twin-cuvette system it is possible to measure stable O_3 and PAN mixing ratios over long time periods under controlled environmental conditions. The resolution of the mixing ratio difference was quite high, so that even small differences in the range of a few hundred ppt in O_3 and several ppt in PAN could be differentiated in the measurement data (see Sect. 3.1.1, Table 2). Especially for the investigations on the flux partitioning, i.e., the discrimination between stomatal and non-stomatal deposition of O_3 and PAN, a measurement system with high precision to resolve the mixing ratio difference was required. The mixing ratios used during the long-term flux experiments (57 ppb for O_3 and 280 ppt for PAN, see Fig. 9) as well as the mixing ratios inside the sample cuvette (58.8 ppb for O_3 and 307.6 ppt for PAN) were far above the measured detection limits of the twin-cuvette setup (0.9 ppb for O_3 and 1.3 ppt for PAN, see also Table 3), but representative for ambient conditions. The good resolution of the mixing ratio difference between both cuvettes (see Table 2) was due to the very high precision and stability of the measured mixing ratio signal of O_3 and PAN within

Figure 13. Relationship between the measured stomatal conductance $g_{s,meas}$ and calculated stomatal conductance $g_{s,calc}$ to O_3 (left) and PAN (right).

Figure 14. Relationship between relative humidity and electrical leaf surface conductance.

Table 6. Comparison of O_3 and PAN flux between a single-cuvette and dual cuvette measurement system.

Trace gas	Method	Flux ($nmol\,m^{-2}\,s^{-1}$)
O_3	Single cuvette	1.2 ± 0.2
	Dual cuvette	1.1 ± 0.1
PAN	Single cuvette	$4.2 \times 10^{-3} \pm 3.0 \times 10^{-4}$
	Dual cuvette	$3.3 \times 10^{-3} \pm 2.0 \times 10^{-4}$

4.1.2 ATRAHS

To investigate the uptake of trace gases by plant leaves under controlled laboratory conditions, the simulation of environmental parameters such as light, temperature, and relative humidity inside the cuvettes is essential (Niinemets et al., 2011). For the non-stomatal deposition of O_3 and PAN to plant leaves, the influence of liquid films on leaf surfaces to the deposition of O_3 and PAN is discussed as an important factor (Fuentes and Gillespie, 1992; Shepson et al., 1992; Doskey et al., 2004; Moravek et al., 2015). To study the effect of different moisture levels on the non-stomatal deposition, the humidity inside the dynamic cuvettes system has to be changed with reliable accuracy. Various methods to humidify the cuvette air exist, which was presented in previous studies. Dynamic plant cuvettes for laboratory studies from Kesselmeier et al. (1996, 1998) and Breuninger et al. (2012) use air humidification to create a proper environmental growth condition for the plant inside the cuvette. Thereby, the dry air stream was flushed through a water tank for humidification. A regulation of the inner relative humidity was not provided. However, many other studies such as Neubert et al. (1993), Fares et al. (2008) and Wildt et al. (1997) did not specify the humidification system used. Thereby, the water vapor content inside the cuvette was defined by the plant transpiration. In the cuvette system from Stokes et al. (1993) and Behrendt et al. (2014), the relative humidity inside the cuvette could be controlled by mixing a

the cuvette system. As these mixing ratio differences are used to calculate the fluxes, the fluxes could be determined with a high sensitivity as well. Furthermore, the twin-cuvette system was tested to be a more precise method to perform flux measurements with reactive trace gas species under controlled laboratory conditions than a single-cuvette system. As shown in Table 6, the O_3 and PAN fluxes with a single-cuvette system were calculated as $1.2 \pm 0.2\,nmol\,m^{-2}\,s^{-1}$ for O_3 and $4.2 \pm 0.3\,pmol\,m^{-2}\,s^{-1}$ for PAN. This indicate some overestimation at least for PAN when relying on inlet/outlet measurements with a single-cuvette system. The flux overestimation with a single-cuvette system is caused by an underestimation of the O_3 and PAN deposition on the cuvette foil, which had to be considered during the flux calculation with the single-cuvette system. For the twin-cuvette system, such a correction is not needed.

bypass stream of wet air into the dry air stream. Normally, these systems (depending on the relative flow rates of the dry and humidified stream) cannot reach very high values of RH. Additionally, two MFCs are necessary for each cuvette to control both (dry and humid) additive air streams. Thereby, the precision of the adjusted humidity is dependent on the precision of all involved MFCs. Compared to all these methods, ATRAHS provides an opportunity to humidify the air stream directly. With this system, the humidity level inside the cuvettes could be held constant and regulated with high precision. Furthermore, the automatic water-filling mechanism avoids an interruption of the long-term measurements improving the performance of the entire measurement system and preventing data gaps. Due to the mechanical float valve, the water-filling process occurred continuously, so that the change of the water level inside the humidifier tank was very limited. In this case, the regulation of the humidity level by changing the heat temperature was very efficient due to the small volume of new water, which was filled to the humidifier tank. Additionally, only one MFC was needed for each cuvette when using ATRAHS. Thereby, a high precision of 0.3 % of the adjusted relative humidity could be achieved. The only limits are the range of the humidification, which was dependant on the water temperature of the humidifier, thus limited by the environmental temperature. The lowest adjustable humidification limit was 50 % at a temperature of 19.5 °C and flow rate of 20 L min^{-1}, which was sufficient for our experiments. To achieve the range below 50 % RH with ATRAHS in the current setup, a cooling system would be needed for the humidifier tank to receive a lower water temperature.

4.2 Flux measurements under laboratory conditions

During the long-term experiment a decreasing trend of the water flux was observed over the measurement period, which became constant after 10 days. This effect might be due to the acclimatization process of the plant by changing the location from the greenhouse to the plant cabinet. From previous studies it is known that plant samples need a significant amount of days to adapt for changes in temperature, light intensity and relative humidity (Kesselmeier et al., 1998). Also, as the measurement was performed in October, the onset of winter stress could have played a role in the reduction of the water flux with time as it also effects the transpiration rate (Oh and Koh, 2014). A similar reducing trend could also be observed for the deposition fluxes of O$_3$ and PAN. To suppress annual behaviors such as the winter dormancy, the plant samples would have had to be grown under very constant environmental condition, which was not possible in our case, considering a growing time of 3 years. During the light periods, the determined deposition velocities ranged for O$_3$ from 0.66 to 1.06 mm s^{-1}, which is comparable to Fares et al. (2008). Values for PAN of 0.32–0.48 mm s^{-1} were comparable to the study of Teklemariam and Sparks (2004) (see

Table 1). During the dark periods the deposition velocity of O$_3$ was slightly higher than that of PAN (see Sect. 3.2.1). As the leaf stomata were closed under dark conditions, the O$_3$ deposition is most likely associated with non-stomatal uptake on the leaf surface. Fuentes and Gillespie (1992) showed that the deposition of O$_3$ can be reinforced by liquid water films on the leaf surface, which could be formed at high humidity. For example, Burkhardt and Eiden (1994) found that the relationship between humidity and electrical surface conductance of the plant leaves is due to the dissolution of ammonia and migration of ions in the liquid water film along the leaf surface of the plant. Further, atmospheric particles deposited on the leaf surface are likely to become deliquescent within the water vapor transpired by the leaf (Burkhardt et al., 2001). For these reasons we exposed the plant to ambient air, just outside the institute, to simulated natural conditions. Atmospheric particles could deposit on the plant leaves and increase the electrical surface conductance with rising ambient humidity inside the cuvette (see Sect. 3.2.4). The ABA experiment showed a clear effect of ABA on the leaf stomata closure in regard to the deposition fluxes of O$_3$ and PAN. The linear relationship between the measured and calculated stomatal conductance to O$_3$ ($R_{pearson} = 0.99$; CI$_{95\%} = 0.07$) and PAN ($R_{pearson} = 0.91$; CI$_{95\%} = 0.1$) shows predominantly stomatal uptake of both gas species, which agrees with results of previous studies (Okano et al., 1990; Sparks et al., 2003; Doskey et al., 2004; Fares et al., 2008, 2010). For the calculation of $g_{s,meas}$ we assumed that vmr$_{int,leaf}$ (O$_3$) was close to zero (Laisk et al., 1989; Doskey et al., 2004) as well as for PAN (see Sect. 2.2.5, Eq. 10). In case of O$_3$ at < 50 % RH, the linear slope of 0.98 ± 0.01 indicates that there is no additional internal leaf resistance and surface deposition of O$_3$ such as liquid water films as it was reported by Fuentes and Gillespie (1992). That O$_3$ is rapidly decomposed in cell walls and plasmalemma has already been reported by Laisk et al. (1989). The absence of epicuticular deposition might have been caused by the low relative humidity of 40 % within the cuvettes during this experiment. As a consequence, we could conclude that below 40 % RH, the surface deposition had no important contribution to the total O$_3$ deposition. As observed in Fig. 14, the value of RH$_{crit}$, the humidity level where the formation of the leaf surface water film starts, was found at 60 %. However, Jud et al. (2016) observed a contribution of semi-volatile organic compounds, in this case diterpenes of *Nicotiana tabacum*, to non-stomatal sinks of O$_3$. These observations demonstrated that special structures or organs can exist on the plant surface as in the case of glandular trichomes of *Nicotiana tabacum*, which may release stored volatile organic compounds impacting gas phase chemistry. Such an incidence may act as a contribution to non-stomatal O$_3$ sinks which should be kept in mind, especially for highly reactive sesquiterpenes, which may contribute by ozonolysis within the canopy (Jardine et al., 2011). However, sequiterpene emission from healthy holm oak is negligible (Staudt and Houtellier, 2007). Further-

more, based on the results of our experiment under laboratory conditions, we conclude that due to the short residence time of 3.4 minutes, a contribution of gas phase reactions with O_3 and monoterpenes from the internal leaf tissue to the non-stomatal deposition is low. An effect of ABA on the monoterpene production would affect the monoterpene synthesis on an even lower level. The gas phase reaction with O_3 is an aspect of non-stomatal O_3 deposition which would become important when discussing a complete forest ecosystem. For PAN the slope ($m = 0.64 \pm 0.02$) was lower than unity. This indicates an additional resistance to PAN deposition, which might be caused by limited uptake and transport in the leaves mesophilic cells. Therefore, the internal leaf PAN mixing ratio should not be zero as a result of the mesophyllic resistance for PAN, which is assumed to be higher than for O_3 (Sparks et al., 2003; Doskey et al., 2004; Teklemariam and Sparks, 2004; Moravek et al., 2015). The results from further detailed investigations on the non-stomatal deposition of PAN and O_3 to leaf surfaces will be presented in a subsequent publication.

5 Conclusions

By using a comparative measurement technique with a twin-cuvette system, we are able to perform trace gas exchange measurements with high precision and resolution of the measured trace gas mixing ratios. In our experimental setup, it is possible to control multiple environmental parameters such as light, temperature, trace gas mixing ratio and relative humidity inside the dynamic cuvettes. The comparison of fluxes between a single and the twin – cuvette system revealed an overestimation of fluxes by the single-cuvette system for both O_3 (8.3 %) and PAN (21.4 %), which is due to unconsidered effects of wall deposition. Consequently, the dual cuvette system represents a more precise method to perform flux measurements with reactive trace gas species under controlled laboratory conditions. Furthermore, with ATRAHS the relative humidity inside the cuvette could be controlled with a high precision of 0.3 %. According to our experimental data, ATRAHS is suitable for cuvette systems operated with higher flow rates ($> 20\,L\,min^{-1}$), but it could be also possible to use for lower flow rates ($> 5\,L\,min^{-1}$), and where humidity values up to 100 % are required. Due to the automatic water-filling mechanism, an interruption to refill the water for humidification during long-term measurements is not necessary, which improves the performance of the entire measurement system and prevents data gaps. O_3 and PAN exchange fluxes were determined with *Quercus ilex* during a long-term experiment of 2 weeks under controlled laboratory conditions. The deposition velocity ratio of O_3 and PAN was determined as 0.45 ± 0.04. By using O_3 mixing ratios between 32 and 105 ppb and PAN mixing ratios between 100 and 350 ppt a linear dependency of the O_3 flux as well as the PAN flux to its ambient mixing ratio could be observed. Furthermore, we are able to observe and characterize the for-

mation of a water film on the leaf surface by measuring its electrical surface conductance with the leaf wetness sensor. An exponential relationship was observed between the electrical surface conductance and the ambient humidity, with a critical value of the relative humidity of 60 %. The combination of all these features of the presented twin-cuvette system will give the opportunity to investigate further questions as flux partitioning between stomatal and non-stomatal deposition of O_3 and PAN and the influence of liquid films on a leaf surface.

References

Altimir, N., Kolari, P., Tuovinen, J.-P., Vesala, T., Bäck, J., Suni, T., Kulmala, M., and Hari, P.: Foliage surface ozone deposition: a role for surface moisture?, Biogeosciences, 3, 209–228, doi:10.5194/bg-3-209-2006, 2006.

Atkinson, R., Baulch, D. L., Cox, R. A., Crowley, J. N., Hampson, R. F., Hynes, R. G., Jenkin, M. E., Rossi, M. J., Troe, J., and IUPAC Subcommittee: Evaluated kinetic and photochemical data for atmospheric chemistry: Volume II – gas phase reactions of organic species, Atmos. Chem. Phys., 6, 3625–4055, doi:10.5194/acp-6-3625-2006, 2006.

Bakr, E. M.: A New Software for Measuring Leaf Area, and Area Damaged by *Tetranychus Urticae* Koch, Blackwell Verlag, Berlin, vol. 129, 173–175, 2005.

Behrendt, T., Veres, P. R., Ashuri, F., Song, G., Flanz, M., Mamtimin, B., Bruse, M., Williams, J., and Meixner, F. X.: Characterisation of NO production and consumption: new insights by an improved laboratory dynamic chamber technique, Biogeosciences, 11, 5463–5492, doi:10.5194/bg-11-5463-2014, 2014.

Bevington, P. R. and Robinson, D. K.: Data Reduction and Error Analysis for the Physical Sciences, 3rd edn., McGraw-Hill, New York, ISBN: 0-07-247227-8, 2002.

Bonn, B., Sun, S., Haunold, W., Sitals, R., van Beesel, E., dos Santos, L., Nillius, B., and Jacobi, S.: COMPASS –COMparative Particle formation in the Atmosphere using portable Simulation chamber Study techniques, Atmos. Meas. Tech., 6, 3407–3423, doi:10.5194/amt-6-3407-2013, 2013.

Breuninger, C., Oswald, R., Kesselmeier, J., and Meixner, F. X.: The dynamic chamber method: trace gas exchange fluxes (NO, NO_2, O_3) between plants and the atmosphere in the laboratory and in the field, Atmos. Meas. Tech., 5, 955–989, doi:10.5194/amt-5-955-2012, 2012.

Burkhardt, J. and Eiden, R.: Thin water films on coniferous needles, Atmos. Environ., 28, 2001–2011, 1994.

Burkhardt, J. and Gerchau, J.: A new device for the study of water-vapor condensation and gaseous deposition to plant-surfaces and particle samples, Atmos. Environ., 28, 2012–2017, 1994.

Burkhardt, J., Koch, K., and Kaiser, H.: Deliquescence of deposited atmospheric particle on leaf surfaces, Water, Air, Soil Pollut., Focus, 1, 313–321, 2001.

Chaparro-Suarez, I. G., Meixner, F. X., and Kesselmeier, J.: Nitrogen dioxide (NO_2) uptake by vegetation controlled by atmospheric concentrations and plant stomatal aperture, Atmos. Environ., 45, 5742–5750, 2011.

Doskey, P. V., Kotamarthi, V. R., Fukui, Y., Cook, D. R., Breitbeil, F. W., and Wesely, M. L.: Air–surface exchange of peroxyacetyl nitrate at a grassland site, J. Geophys. Res.-Atmos., 109, D10310, doi:10.1029/2004JD004533, 2004.

Fares, S., Loreto, F., Kleist, E., and Wildt, J.: Stomatal uptake and stomatal deposition of ozone in isoprene and monoterpene emitting plants, Plant Biol., 10, 44–54, 2008.

Fares, S., Park, J. H., Ormeno, E., Gentner, D. R., McKay, M., Loreto, F., Karlik, J., and Goldstein, A. H.: Ozone uptake by citrus trees exposed to a range of ozone concentrations, Atmos. Environ., 44, 3404–3412, doi:10.1016/j.atmosenv.2010.06.010, 2010.

Fuentes, J. D. and Gillespie, T. J.: A gas-exchange system to study the effects of leaf surface wetness on the deposition of ozone, Atmos. Environ., 26, 1165–1173, 1992.

Garland, J. A. and Penkett, S. A.: Absorption of peroxy acetyl nitrate and ozone by natural surfaces, Atmos. Environ., 10, 1127–1131, 1976.

Goff, J. A. and Gratch, S.: Low-pressure properties of water from -160 to 212 F, T. Am. Soc. Heat. Ventil. Engin., 52, 95–121, 1946.

Gut, A., Scheibe, M., Rottenberger, S., Rummel, U., Welling, M., Ammann, C., Kirkman, G. A., Kuhn, U., Meixner, F. X., Kesselmeier, J., Lehmann, B. E., Schmidt, W., Müller, E., and Piedade, M. T. F.: Exchange fluxes of NO_2 and O_3 at soil and leaf surfaces in an Amazonian rain forest, J. Geophys. Res.-Atmos., 107, 8060, doi:10.1029/2001JD000654, 2002.

Hill, A. C.: Vegetation: a sink for atmospheric pollutants, JAPCA J. Air Waste Ma., 21, 341–346, 1971.

Horst, T. W. and Weil, J. C.: How far is far enough – The fetch requirements for micrometeorological measurement of surface fluxes (Vol 11, PG 1018, 1994), J. Atmos. Ocean. Tech., 12, 447–447, 1995.

Jardine, K., Yañez Serrano, A., Arneth, A., Abrell, L., Jardine, A., Artaxo, P., Alves, E., Kesselmeier, J., Taylor, T., Saleska, S., and Huxman, T.: Ecosystem-scale compensation points of formic and acetic acid in the central Amazon, Biogeosciences, 8, 3709–3720, doi:10.5194/bg-8-3709-2011, 2011.

Jud, W., Fischer, L., Canaval, E., Wohlfahrt, G., Tissier, A., and Hansel, A.: Plant surface reactions: an opportunistic ozone defence mechanism impacting atmospheric chemistry, Atmos. Chem. Phys., 16, 277–292, doi:10.5194/acp-16-277-2016, 2016.

Kesselmeier, J., Schäfer, L., Ciccioli, P., Brancaleoni, E., Cecinato, A., Frattoni, M., Foster, P., Jacob, V., Denis, J., Fugit, J. L., Dutaur, L., and Torres, L.: Emission of monoterpenes and isoprene from a Mediterranean oak species Quercus ilex L measured within the BEMA (Biogenic Emissions in the Mediterranean Area) project, Atmos. Environ., 30, 1841–1850, 1996.

Kesselmeier, J., Bode, K., Gerlach, C., and Jork, E. M.: Exchange of atmospheric formic and acetic acids with trees and crop plants under controlled chamber and purified air condition, Atmos. Environ., 32, 1765–1775, 1998.

Kruit, R. J. W., Jacob, A. F. G., and Holtslaga, A. A. M.: Measurements and estimates of leaf wetness over agricultural grassland for dry deposition modeling of trace gases, Atmos. Environ., 42, 5304–5316, 2008.

Kulmala, M., Hienola, J., Pirjola, L., Vesala, T., Shimmo, M., Altimir, N., and Hari, P.: A model for NO_x-O_3-terpene chemistry in chamber measurements of plant gas exchange, Atmos. Environ, 33, 2145–2156, 1999.

Laisk, A., Kull, O., and Moldau, H.: Ozone concentration in leaf intercellular air space is close to zero, Plant Physiol., 90, 1163–1167, 1989.

Marrero, T. R. and Mason, E. A.: Gaseous diffusion coefficients, J. Phys. Chem. Ref. Data, 1, 3–110, 1972.

Moravek, A., Foken, T., and Trebs, I.: Application of a GC-ECD for measurements of biosphere-atmosphere exchange fluxes of peroxyacetyl nitrate using the relaxed eddy accumulation and gradient method, Atmos. Meas. Tech., 7, 2097–2119, doi:10.5194/amt-7-2097-2014, 2014.

Moravek, A., Stella, P., Foken, T., and Trebs, I.: Influence of local air pollution on the deposition of peroxyacetyl nitrate to a nutrient-poor natural grassland ecosystem, Atmos. Chem. Phys., 15, 899–911, doi:10.5194/acp-15-899-2015, 2015.

Mudelsee, M.: Estimating Pearson's correlation coefficient with bootstrap confidence interval from serially dependent time series, Math. Geol., 35, 651–665, 2003.

Neubert, A., Kley, D., Wildt, J., Segschneider, H. J., and Forstel, H.: Uptake if NO, NO_2 and O_3 by sunflower (*Helianthus-annuus* L.) and Tabacco plants (*Nicotiana-tabacum*-L) – dependence on stomatal conductivity, Atmos. Environ., 27, 2137–2145, 1993.

Niinemets, Ü., Kuhn, U., Harley, P. C., Staudt, M., Arneth, A., Cescatti, A., Ciccioli, P., Copolovici, L., Geron, C., Guenther, A., Kesselmeier, J., Lerdau, M. T., Monson, R. K., and Peñuelas, J.: Estimations of isoprenoid emission capacity from enclosure studies: measurements, data processing, quality and standardized measurement protocols, Biogeosciences, 8, 2209–2246, doi:10.5194/bg-8-2209-2011, 2011.

Oh, S. and Koh, S. C.: Photosystem II photochemical efficiency and photosynthetic capacity in leaves of tea plant (Camellia sinensis L.) under winter stress in the field, Hortic. Environ. Biotechnol., 55, 363–371, 2014.

Okano, K., Tobe, K., and Furukawa, A.: Foliar uptake of peroxyacetyl nitrate (PAN) by herbaceous species varying in susceptibility to this pollutant, New Phytol., 114, 139–145, 1990.

Ortega, J. and Helmig, D.: Approaches for quantifying reactive and low-volatility biogenic organic compound emissions by vegetation enclosure techniques – Part A, Chemosphere, 72, 343–364, doi:10.1016/j.chemosphere.2007.11.020, 2008.

Pape, L., Ammann, C., Nyfeler-Brunner, A., Spirig, C., Hens, K., and Meixner, F. X.: An automated dynamic chamber system

for surface exchange measurement of non-reactive and reactive trace gases of grassland ecosystems, Biogeosciences, 6, 405–429, doi:10.5194/bg-6-405-2009, 2009.

Patz, H. W., Lerner, A., Houben, N., and Volz-Thomas, A.: Validation of a new method for the calibration of peroxy acetyl nitrate (PAN)-analyzers, Gefahrst. Reinhalt. L., 62, 215–219, 2002.

Shepson, P. B., Bottenheim, J. W., Hastie, D. R., and Venkatram, A.: Determination of the relative ozone and PAN deposition velocities at night, Geophys. Res. Lett., 19, 1121–1124, 1992.

Sparks, J, P., Monson, R. K., Sparks, K. L., and Lerdau, M.: Leaf uptake of nitrogen dioxide (NO_2) in a tropical wet forest: implications for tropospheric chemistry, Oecologia, 127, 214–221, 2001.

Sparks, J. P., Roberts, J. M., and Monson, R. K.: The uptake of gaseous organic nitrogen by leaves: a significant global nitrogen transfer process, Geophys. Res. Lett., 30, 2189, doi:10.1029/2003GL018578, 2003.

Staudt, M. and Houtellier, L.: Volatile organic compound emission from holm oak infested by gypsy moth larvae: evidence for distinct responses in damaged and undamaged leaves, Tree Physiology, 27, 1433–1440, 2007.

Stokes, N. J., Lucas, P. W., and Hewitt, C. N.: Controlled environment fumigation chamber for the study of reactive air pollutant effects on plants, Atmos. Environ., 27, 679–683, 1993.

Teklemariam, T. A. and Spaks, J. P.: Gaseous fluxes of peroxyacetyl nitrate (PAN) into plant leaves, Plant Cell Environ., 27, 1149–1158, 2004.

Van Hove, L. W. A., Bossen, M. E., de Bok, F. A. M. and Hooijmaijers, C. A. M.: The uptake of O_3 by poplar leaves: the impact of a long-term exposure to low O_3-concentrations, Atmos. Environ., 33, 907–917, 1999.

Volz-Thomas, A., Xueref, I., and Schmitt, R.: An automatic gas chromatograph and calibration system for ambient measurements of PAN and PPN, Environ. Sci. Pollut. R., 4, 72–76, 2002.

Von Caemmerer, S. and Farquhar, G. D.: Some relationships between the biochemistry of photosynthesis and the gas exchange of leaves, Planta, 153, 376–387, 1981.

Wang, D., Hinckley, T. M., Cumming, A. B., and Braatne, J.: A comparison of measured and modeled ozone uptake into plant leaves, Environ. Pollut., 89, 247–254, 1995.

Wildt, J., Kley, D., Rockel, A., Rockel, P., and Segschneider, H. J.: Emission of NO from several higher plant species, J. Geophys. Res.-Atmos., 102, 5919–5927, 1997.